Rigid Rod-Shaped Polyols: Functional Nonpeptide Models for Transmembrane Proton Channels†

Linnea A. Weiss, Naomi Sakai, Bereket Ghebremariam, Chiyou Ni, and Stefan Matile*

Contribution from the Department of Chemistry, Georgetown University, Washington, D.C. 20057-1227

Received September 5, 1997[⊗]

Abstract: The present study concerns the mode of action of a rigid rod-shaped polyol **1** and the corresponding hexamer **2**. Proton flux mediated by **1** is shown to be strongly favored over metal cations and anions. The modest selectivity for monovalent cations ($Rb^+ > Cs^+ > K^+ > Na^+ \approx Li^+$, Eisenman sequence II) is determined by the dehydration energy and is weakly influenced by the local electric (ionophoric) field. The induction of membrane defects was ruled out by the absence of dye leakage. Structural studies by circular dichroism and fluorescence spectroscopy imply that **1** aggregates in polar and nonpolar solvents, but not in lipid bilayers. Furthermore, it is shown that a very small fraction of **1** adopts a monomeric transmembrane tunnel-like structure which accounts for activity, while the remainder forms inactive self-assemblies. The above results suggest that **1** acts as a functional unimolecular proton wire which mimics the hydrogen-bonded chain mechanism found in bioenergetic systems.

Introduction

Nonpeptide ion channel models[1,2] have been devised over the past two decades in the hope of contributing to the mechanistic understanding of channel proteins on the molecular level, or to develop new pharmaceuticals. Most of the nonpeptide channel models were designed to act either as unimolecular "tunnels" or gramicidin[3] -like, dimerizing "half-pores".[2] In contrast, ion channels formed by peptides and synthetic peptide models[4] function mainly as well-defined self-assemblies which are similar to the "barrel-stave-type" model for the one-sided action of amphotericin B (AmB),[5] and mimic structural aspects of neuronal ion channel proteins.[4]

Previously we have reported the design, synthesis, and preliminary assessment of ion transport activities of a new class of nonpeptide ion channel models, i.e., rigid-rod molecules[6] **1** and **2**, which closely mimic the polyene and polyol subunits of AmB, but lack charged terminal "anchoring" groups (Figure

† Abbreviations: AmB, amphotericin B; CD, circular dichroism; CF, 5(6)-carboxyfluorescein; 5-DOXYL-PC, 1-palmitoyl-2-stearoyl (5-DOXYL)-*sn*-glycero-3-phosphocholine; 12-DOXYL-PC, 1-palmitoyl-2-stearoyl (12-DOXYL)-*sn*-glycero-3-phosphocholine; EYPC, egg yolk phosphatidylcholine; FRET, fluorescence resonance energy transfer; HBC, hydrogen-bonded chain; HPTS, 8-hydroxypyrene-1,3,6-trisulfonic acid; POPG, 1-palmitoyl-2-oleoyl-*sn*-glycero-3-[phospho-*rac*-(1-glycerol)] (sodium salt); SUV, small unilamellar vesicle.

⊗ Abstract published in *Advance ACS Abstracts,* December 1, 1997.

(1) Sakai, N.; Brennan, K. C.; Weiss, L. A.; Matile, S. *J. Am. Chem. Soc.* **1997**, *119*, 8726.

(2) Review on nonpeptide ion channel models: (a) Gokel, G. W.; Murillo, O. *Acc. Chem. Res.* **1996**, *29*, 425. Pertinent references: (b) Murillo, O.; Suzuki, I.; Abel, E.; Murray, C. L.; Meadows, E. S.; Jin, T.; Gokel, G. W. *J. Am. Chem. Soc.* **1997**, *119*, 5540. (c) Meillon, J.-C.; Voyer, N. *Angew. Chem., Int. Ed. Engl.* **1997**, *36*, 967. (d) Sakai, N.; Matile, S. *Tetrahedron Lett.* **1997**, *38*, 2613. (e) Wagner, H.; Harms, K.; Koert, U.; Meder, S.; Boheim, G. *Angew. Chem., Int. Ed. Engl.* **1996**, *35*, 2643. (f) Seebach, D.; Brunner, A.; Bürger, H. M.; Reusch, R. N.; Bramble, L. L. *Helv. Chim. Acta* **1996**, *79*, 507. (g) Fyles, T. M.; Loock, D.; van Straaten-Nijenhuis, W. F.; Zhou, X. *J. Org. Chem.* **1996**, *61*, 8866. (h) Deng, G.; Dewa, T.; Regen, S. L. *J. Am. Chem. Soc.* **1996**, *118*, 8975. (i) Dubowchik, G. M.; Firestone, R. A. *Tetrahedron Lett.* **1996**, *37*, 6465. (j) Tanaka, Y.; Kobuke, Y.; Sokabe, M. *Angew. Chem., Int. Ed. Engl.* **1995**, *34*, 693. (k) Nolte, R. J. M. *Chem. Soc. Rev.* **1994**, 11. (l) Jullien, L.; Lazrak, T.; Canceill, J.; Lacombe, L.; Lehn, J.-M. *J. Chem. Soc., Perkin Trans. 2* **1993**, 1011. (m) Menger, F. M.; Davis, D. S.; Persichetti, R. A.; Lee, J.-J. *J. Am. Chem. Soc.* **1990**, *112*, 2451. (n) Fuhrhop, J.-H.; Liman, U.; Koesling, V. *J. Am. Chem. Soc.* **1988**, *110*, 6840. (o) Tabushi, I.; Kuroda, Y.; Yokota, K. *Tetrahedron Lett.* **1982**, *23*, 4601.

(3) (a) Cornell, B. A.; Braach-Maksvytis, V. L. B.; King, L. G.; Osman, P. D. J.; Raguse, B.; Wieczorek, L.; Pace, R. J. *Nature* **1997**, *387*, 580. (b) Woolley, G. A.; Wallace, B. A. *J. Membr. Biol.* **1992**, *129*, 109. (c) Stankovic, C. J.; Heinemann, S. H.; Delfino, J. M.; Sigworth, F. J.; Schreiber, S. L. *Science* **1989**, *244*, 813.

(4) Selected reviews and references on synthetic peptide channel models: (a) Lear, J. D.; Schneider, J. P.; Kienker, P. K.; DeGrado, W. F. *J. Am. Chem. Soc.* **1997**, *119*, 3212. (b) Clark, T. D.; Ghadiri, M. R. *J. Am. Chem. Soc.* **1995**, *117*, 12364. (c) Grove, A.; Mutter, M.; Rivier, J. E.; Montal, M. *J. Am. Chem. Soc.* **1993**, *115*, 5919. (d) Åckerfeldt, K. S.; Lear, J. D.; Wasserman, Z. R.; Chung, L. A.; DeGrado, W. F. *Acc. Chem. Res.* **1993**, *26*, 191. (e) Åckerfeldt, K. S.; Kim, R. M.; Camac, D.; Groves, J. T.; Lear, J. D.; DeGrado, W. F. *J. Am. Chem. Soc.* **1992**, *114*, 9656. (f) Mutter, M.; Tuchscherer, G. G.; Miller, C.; Altman, K.-H.; Carey, R. I.; Wyss, D. F.; Labhardt, A. M.; Rivier, J. E. *J. Am. Chem. Soc.* **1992**, *114*, 1463.

(5) Review: (a) Bolard, J. *Biochim. Biophys. Acta* **1985**, *864*, 257. Pertinent references: (b) Hartsel, S. C.; Benz, S. K.; Peterson, R. P.; Whyte, B. S. *Biochemistry* **1991**, *30*, 77. (c) Bolard, J.; Legrand, P.; Heitz, F.; Cybulska, B. *Biochemistry* **1991**, *30*, 5707. (d) Hartsel, S. C.; Perkins, W. R.; McGarvey, G. J.; Cafiso, D. S. *Biochemistry* **1988**, *27*, 2656. (e) Kleinberg, M. E.; Finkelstein, A. *J. Membr. Biol.* **1984**, *80*, 257. (f) Vertut-Croquin, A.; Bolard, J.; Chabbert, M.; Gary-Bobo, C. *Biochemistry* **1983**, *22*, 1939. (g) Marty, A.; Finkelstein, A. *J. Gen. Physiol.* **1975**, *65*, 515. (h) De Kruijff, B.; Demel, R. A. *Biochim. Biophys. Acta* **1974**, *339*, 57. (i) Andreoli, T. E. *Kidney Int.* **1973**, *4*, 337.

(6) Selected references on rigid rod molecules: (a) Maddux, T.; Li, W.; Yu, L. *J. Am. Chem. Soc.* **1997**, *119*, 844. (b) Rajca, A.; Safronov, A.; Rajca, S.; Shoemaker, R. *Angew. Chem., Int. Ed. Engl.* **1997**, *36*, 448. (c) Keegstra, M. A.; De Feyter, S.; De Schryver, F.; Müllen, K. *Angew. Chem., Int. Ed. Engl.* **1996**, *35*, 775. (d) Nuding, G.; Vögtle, F.; Danielmeier, K.; Steckhan, E. *Synthesis* **1996**, 71. (e) Li, W.; Fox, M. A. *J. Am. Chem. Soc.* **1996**, *118*, 11752. (f) Ayres, F. D.; Khan, S.; Chapman, O. L. *Tetrahedron Lett.* **1994**, *35*, 8561. (g) Eaton, P. E.; Galoppini, E.; Gilardi, R. *J. Am. Chem. Soc.* **1994**, *116*, 7588. (h) Mehta, G.; Viswanath, M. B.; Kunwar, A. C. *J. Org. Chem.* **1994**, *59*, 6131. (i) Baker, K. N.; Fratini, A. V.; Resch, T.; Knachel, H. C.; Adams, W. W.; Socci, E. P.; Farmer, B. L. *Polymer* **1993**, *34*, 1571. (j) Kaszynski, P.; Friedli, A. C.; Michl, J. *J. Am. Chem. Soc.* **1992**, *114*, 601. (k) Yang, X.; Jiang, W.; Knobler, C. B.; Hawthorne, M. F. *J. Am. Chem. Soc.* **1992**, *114*, 9719. (l) Ashton, P. R.; Brown, G. R.; Isaacs, N. S.; Giuffrida, D.; Kohnke, F. H.; Mathias, J. P.; Slawin, A. M. Z.; Smith, D. R.; Stoddart, J. F.; Williams, D. J. *J. Am. Chem. Soc.* **1992**, *114*, 6330. (m) Zimmerman, H. E.; King, R. K.; Meinhardt, M. B. *J. Org. Chem.* **1992**, *57*, 5484. (n) Bohnen, A.; Heitz, W.; Müllen, K.; Räder, H.-J.; Schenk, R. *Macromol. Chem.* **1991**, *192*, 1679. (o) Lehn, J.-M. In *Frontiers in Supramolecular Organic Chemistry and Photochemistry;* Schneider, H.-J., Dürr, H., Eds.; VCH: Weinheim, 1991; p 1. (l) Feldman, K. S.; Bobo, J. S.; Ensel, S. M.; Lee, Y. B.; Weinreb, P. H. *J. Org. Chem.* **1990**, *55*, 474. (p) Rinke, M.; Güsten, H.; Ache, H. J. *J. Phys. Chem.* **1985**, *90*, 2661. (q) Heitz, W.; Ullrich, R. *Makromol. Chem.* **1966**, *98*, 29. (r) Kern, W.; Ebersbach, H. W.; Ziegler, I. *Makromol. Chem.* **1965**, *83*, 154.

S0002-7863(97)03126-0 CCC: $14.00

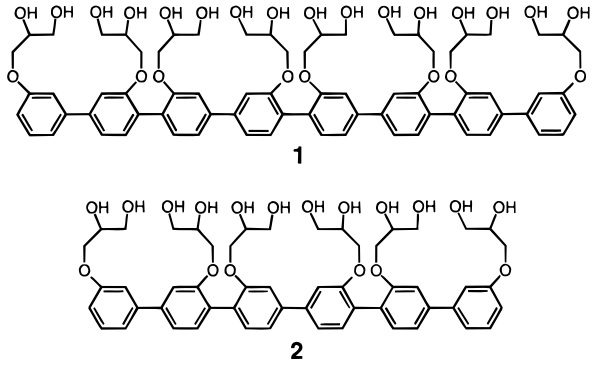

Figure 1. Structures of rigid rod polyols **1** and **2** (diastereomeric mixtures).

1).[1] As in the case of the one-sided action of AmB,[5e] hydrophobic interactions gave rise to length-dependent activity. The structural and mechanistic studies presented in this paper focus on the mode of action of the most active oligomer **1**, having a length (34 Å) which nearly matches the thickness of the hydrophobic part of egg yolk phosphatidylcholine (EYPC) bilayers (ca. 36 Å). These studies allowed us to conclude that **1** acts as a selective, presumably unimolecular proton channel[7] which represents the first nonpeptide channel model of the hydrogen-bonded chain (HBC) mechanism[8] underlying bioenergetic processes. A molecular model of the HBC in the proposed active conformer **1a** is shown in Figure 2B.

Hydrogen-bonded chain mechanisms have attracted a great deal of attention since the pioneering studies of Onsanger, because they are thought to account for the function of proton channels which are crucial in membrane bioenergetics.[8] HBC mechanisms in proteins are two-step processes, "hop-and-turn" (Figure 3), in which the net translocation of a proton occurs through successive hypothetical "hops" (Figure 3A) followed by sequential reorienting "turns" (Figure 3B) of the new O−H bonds to assume the initial configuration, which allows another proton to enter the proton wire. HBC proton wires have been identified in bacterial cytochrome *c* oxidase[9] and in bacteriorhodopsin.[10] Considering the biological significance of proton wires and the involved questions (e.g., the kinetic competence of HBC mechanisms in bioenergetics),[8] it appears surprising that the design and study of nonpeptide proton wires has not received much attention so far.[11]

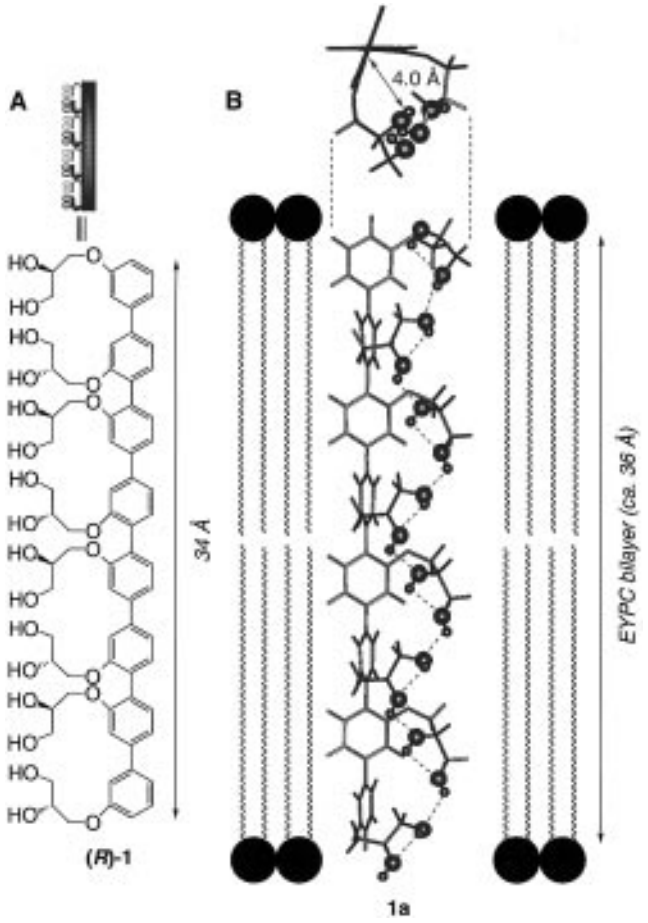

Figure 2. In-scale structure of **(*R*)-1** (A) and 3D-drawing (using Cerius2, Molecular Simulations, Inc.), (B) of the proposed active conformer **1a** of **(*R*)-1** shown in side and top views. Black circles indicate the OH groups; dotted lines (H-bonds) are added to illustrate the HBC. Molecular models further indicate that any diastereomer of **(*R*)-1** can adopt similar conformations and form an intramolecular HBC. Note that conformational changes by rotation around the phenyl−phenyl single bonds are possible in this model without disconnection of the HBC. A helical HBC would be the other conformational extreme relative to the facial amphiphile shown here.

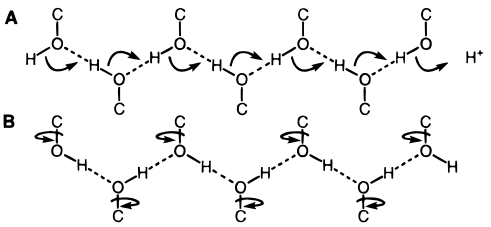

Figure 3. Hydrogen-bonded chain (HBC) mechanism: (A) "hop" and (B) "turn".

Results and Discussion

Proton Selectivity. Ion transport activities were evaluated with uniformly-sized small unilamellar vesicles (SUVs, diameter 68 ± 3 nm) composed of fresh EYPC having a hydrophobic part (36 Å)[12] which approximately matches the length of octamer **1** (34 Å).[1] EYPC-SUVs containing entrapped HPTS (8-hydroxypyrene-1,3,6-trisulfonic acid) were prepared by the dialytic detergent removal technique (100 mM HEPES, 100 mM KCl or NaCl, pH 7.0).[13] In the presence of a transmembane pH gradient, changes in internal pH can be monitored by

(7) Defect induction, ion channel, and mobile ion carrier mechanisms are commonly considered to be three distinct modes of action, although they may be seen as a continuum characterized by decreasing transport rates and increasing selectivity. The term "ion channel" is traditionally reserved for electrophysiologial experiments. Since results from planar bilayer lipid membranes and SUVs cannot be correlated, and since SUVs are not accessible for bilayer clamp experiments, *the term "ion channel" is not defined for SUVs*, the system of choice for structural and mechanistic studies using spectroscopic methods. For consistancy with its traditional definition, the term "ion channel" as used in this text may thus be read as "ion channel-like" or "ion tunnel".[2a]

(8) Review: (a) Nagle, J. F.; Tristram-Nagle, S. *J. Membr. Biol.* **1983**, *74*, 1. Recent pertinent reference: (b) Pomès, R.; Roux, B. *Biophys. J.* **1996**, *71*, 19.

(9) Iwata, S.; Ostermeier, C.; Ludwig, B.; Michel, H. *Nature* **1995**, *376*, 660.

(10) Lanyl, J. K. *Nature* **1995**, *375*, 461.

(11) Peptide-based proton channel models which may follow a HBC-mechanism judging from the serine-rich pore have been reported by DeGrado and co-workers.[4e] Due to the lack of H-bond donors, an HBC-mechanism cannot account for the recently reported proton transport mediated by a nonpeptide polyamine chain.[2i] A model complex for a hydrogen-bonded chain in the active center of alcohol dehydrogenases was reported. Brzezinski, B.; Urjasz, H.; Zundel, G.; Bartl, F. *Biochem. Biophys. Res. Commun.* **1997**, *231*, 473.

(12) (a) Kleinfeld, A. M. *Curr. Top. Membr. Transp.* **1987**, *29*, 1. (b) Caffrey, M.; Feigenson, G. W. *Biochemistry* **1981**, *20*, 1949.

(13) (a) Zumbühl, O.; Weder, H. G. *Biochim. Biophys. Acta* **1981**, *640*, 252. (b) Mimms, L. T.; Zampighi, G.; Nozaki, Y.; Tanford, C.; Reynolds, J. A. *Biochemistry* **1981**, *20*, 833.

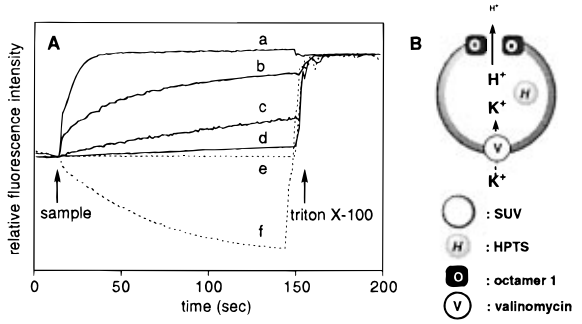

Figure 4. Octamer **1**-induced ion permeability in the presence of valinomycin. (A) Change in fluorescent intensity ($(I_t - I_0)/(I_\infty - I_0)$, $\lambda_{em} = 510$ nm, $\lambda_{ex} = 460$ nm) of vesicle-entrapped HPTS as a function of time after the addition of 24 pmol of valinomycin and/or 40 nmol of octamer **1** (pH_{in} 7.0, pH_{out} 7.6; 100 mM MCl, M = Na or K, 100 mM HEPES buffer was used unless otherwise indicated). (a) **1** with valinomycin, $M_{out} = K$, $M_{in} = Na$, + 0.05 mM internal KCl. (b) **1** with valinomycin, $M_{out} = M_{in} = K$. (c) **1**, $M_{out} = M_{in} = K$ (very similar curves for **1** without valinomycin were obtained at the other salt concentrations used). (d) Valinomycin, $M_{out} = M_{in} = K$ ($M_{out} = K$, $M_{in} = Na$, 0.05 mM internal KCl, valinomycin gave the same curve). The small increase in intensity could be attributed to K^+/H^+ antiport by valinomycin. (e) Valinomycin, $M_{out} = Na$, $M_{in} = K$, + 0.05 mM external KCl. (f) **1** with valinomycin, $M_{out} = Na$, $M_{in} = K$, + 0.05 mM external KCl. (B) Schematic representation of the transport experiment shown in curve b.

emission of the intravesicular HPTS.[14] The observed rate of internal pH change is limited either by the slowest ion transport rate of facilitated H^+/M^+ or OH^-/Cl^- exchange or by the formation rate of the active suprastructures.[15] More information can be obtained from this method by addition of selective ion carriers. For instance, the observed unchanged flux rates in the presence of a proton carrier indicated that proton transport is not rate limiting for the transmembrane ion exchange process mediated by rigid rod polyol **1**.[1]

Evidence for significant $H^+ > K^+$ selectivity of **1** was obtained using a similar strategy; internal pH changes were monitored by the same method in the presence of the selective potassium carrier valinomycin (Figure 4B). While 12 nM valinomycin without polyol **1** gave a minor increase in internal HPTS emission (Figure 4A, curve d), the apparent flux rate mediated by **1** was 16-fold higher when valinomycin was present (Figure 4A, curves b and c). Since no further chemical or electrical gradients besides the difference in internal and external pH affect this system ($[K^+_{in}] = [K^+_{out}] = 100$ mM), the observed rate increase in the presence of valinomycin implies that octamer **1** acts under these conditions as a H^+/K^+ exchanger with significant $H^+ > K^+$ selectivity (Figure 4B). This significant proton selectivity of octamer **1** is best explained by the previously discussed HBC mechanism (Figure 3).

Further effects of additional chemical and electrical gradients on the valinomycin-supported ion exchange mediated by **1** are consistent with this interpretation. For instance, a potassium gradient and a valinomycin-induced stable Nernst potential[16] ($\psi = +190$ mV, $[Na^+_{in}] = [K^+_{out}] = 100$ mM, $[K^+_{in}] = 0.05$ mM) supporting the proton flux along the applied pH gradient strongly accelerated polyol-mediated H^+ efflux (Figure 4A, curve a). Reversed sodium and potassium ion gradients ($[K^+_{in}] = [Na^+_{out}] = 100$ mM, $[K^+_{out}] = 0.05$ mM) lead to a decrease in internal pH, indicating a polyol-mediated uphill proton flux driven by the potassium gradient and membrane potential of $\psi = -190$ mV (Figure 4A, curve f).[17]

Surprisingly, a 20-fold decreased concentration of polyol **1** (from 20 to 1 μM) gave a 3.2-fold lower ion exchange rate (Table 1, entries 4−6). Assuming that ≤100% of the octamer **1** present adopts an active structure at a concentration of 1 μM, this unusual concentration dependence indicates that, as is the case with the ion channel-forming polypeptide alamethicin,[3b] a minor part (≤16%) of polyol **1** accounts for the activity at 20 μM, while more than 84% is inactive. A relatively increased activity at low concentrations further suggests that the active structure of polyol **1** is monomeric (i.e., conformer **1a**, Figure 5), and that an inactive self-assembly of **1** (i.e., **1b**, Figure 5) is dominant at higher concentrations. The resulting incorporation mechanism shown in Figure 5 was further investigated by circular dichroic (CD) and fluorescence measurements as discussed below.

Selectivity for Group IA and Divalent Cations. The above finding that octamer **1** acts with high $H^+ > K^+$ selectivity offered a convenient method to determine the selectivity of **1** for group IA and divalent cations. The same EYPC-SUVs used above were isoosmotically diluted with M_mCl_n solutions, and the external pH was increased. As a result, parallel H^+ and Na^+ gradients opposing a M^{n+} gradient are established (Figure 6A). Since polyol **1** acts with $H^+ > Na^+$ selectivity, an H^+/M^{n+} exchange with partially[15] rate limiting M^{n+} influx will occur. The relative rate constants (i.e., $k_{M^{n+}}/k_{Na^+}$) reveal a modest $Rb^+ > Cs^+ > K^+ > Na^+ \approx Li^+ > Mg^{2+} \geq Ca^{2+}$ selectivity for the transmembrane ion transport mediated by polyol **1** (Table 1, entries 1 and 7−12). Note that the relative rate constant for Na^+ (i.e., k_{Na^+}/k_{Na^+}) cannot be directly compared to the other values because of different experimental conditions; the presence of two metal cation gradients should slightly accelerate the rate-limiting Na^+ flux.

The selectivity observed for group IA cations follows the Eisenman sequence II. The Eisenman theory of ion permeability[18] invokes a balance of the desolvation energy of the ion and the binding energy between the ion and binding sites. Sequence II indicates that the selectivity of polyol **1** is mainly determined by cation desolvation, i.e., weak potential cation−π[19] and cation−oxygen interactions. Weak binding sites and weak selectivity between group IA and divalent cations (and anions) support a channel mechanism[7] and disfavor a mobile carrier mechanism.[2g]

Anion Transport. In order to verify whether or not **1** is capable of mediating anion exchange, the same HPTS-containing SUVs were isoosmotically diluted with Na_nX_m solutions (X = Br, SO_4), and the external pH was increased. In contrast to the system used for cations, the resulting anion gradient runs parallel to the OH^- gradient (Figure 6B). The observed increased overall rates for X = Br/SO_4 (Table 1, entries 13 and 14) thus indicate accelerated OH^-/Cl^- exchange. These changes demonstrate polyol-mediated anion transport. Since there is no experimental evidence that OH^- transport is as preferred as proton transport, further conclusions about anion selectivity sequences are impossible at this stage. However, it should be

(14) In all the experiments conducted with HPTS, the intensity change was confirmed to be the consequence of the pH change by the comparison of the excitation spectra of HPTS, before and after the addition of the samples; a pH increase resulted in an increase in excitation intensity at 460 nm and a decrease in excitation intensity at 405 nm, and *vice versa* for a pH decrease. (a) Kano, K.; Fendler, J. H. *Biochim. Biophys. Acta* **1978**, *509*, 289. (b) Venema, K.; Gibrat, R.; Grouzis, J.-P.; Grignon, C. *Biochim. Biophys. Acta* **1993**, *1146*, 87.

(15) Hervé, M.; Cybulska, B.; Gery-Bobo, C. M. *Eur. Biophys. J.* **1985**, *12*, 121.

(16) (a) Woolley, G. A.; Deber, C. M. *Biopolymers* **1989**, *28*, 267; (b) Woolley, G. A.; Kapral, M. K.; Deber, C. M. *FEBS Lett.* **1987**, *224*, 337. (c) Weiss, L. A., Matile, S. Unpublished results.

(17) Under the identical conditions, ion channel-forming gramicidin D showed a potential independent proton efflux.[16c]

(18) Eisenman, G.; Horn, R. *J. Membr. Biol.* **1983**, *76*, 197.

(19) Dougherty, D. A. *Science* **1996**, *271*, 163.

Table 1. Ion Transport Mediated by Rigid Rod Polyol **1**

entry	[polyol **1**] [μM]	membrane composition	[internal salt] (100 mM)	[external salt] (100 mM)	[valinomycin] (12 nM)	relative rate[a]
1	20	EYPC	NaCl	NaCl	−	1.00
2	20	EYPC	KCl	KCl	−	1.00
3	20	EYPC	KCl	KCl	+	16.00
4	20	EYPC	NaCl[b]	KCl	+	33.00
5	5	EYPC	NaCl[b]	KCl	+	17.60
6	1	EYPC	NaCl[b]	KCl	+	10.27
7	20	EYPC	NaCl	LiCl	−	1.00
8	20	EYPC	NaCl	KCl	−	1.06
9	20	EYPC	NaCl	RbCl	−	1.25
10	20	EYPC	NaCl	CsCl	−	1.14
11	20	EYPC	NaCl	$CaCl_2$	−	0.82
12	20	EYPC	NaCl	$MgCl_2$	−	0.83
13	20	EYPC	NaCl	NaBr	−	1.08
14	20	EYPC	NaCl	Na_2SO_4	−	1.57
15	20	EYPC/Chol[c]	NaCl	KCl	−	1.43
16	20	EYPC/Erg[d]	NaCl	KCl	−	1.56
17	20	POPG	NaCl	KCl	−	4.23
18	5	POPG	NaCl	KCl	−	1.42
19	1	POPG	NaCl	KCl	−	0.76

[a] Relative rate to that of entry 1 ($k = 13.5 \times 10^{-4}$ s^{-1}). [b] +0.05 mM KCl. [c] 25 mol % cholesterol. [d] 25 mol % ergosterol.

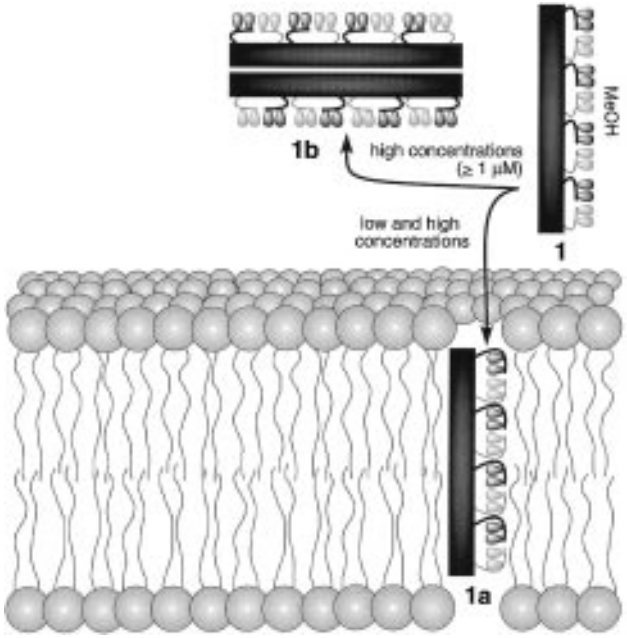

Figure 5. Concentration dependent mechanism of action of rigid rod polyol **1**.

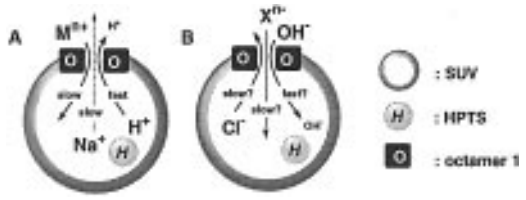

Figure 6. Schematic representation of the transport experiments used to determine cation (A, entries 7−12 of Table 1) and anion selectivity (B, entries 13 and 14 of Table 1).

noted that an HBC mechanism theoretically also applies for OH^- (compare Figure 3).

Bilayer Membrane Recognition. The dependence of polyol **1** activity on lipid bilayer composition was evaluated with EYPC-SUVs containing 25 mol % cholesterol or ergosterol and 1-palmitoyl-2-oleoyl-*sn*-glycero-3-[phospho-*rac*-(1-glycerol)] (POPG)-SUVs.[20] In all cases, an increase in the apparent flux rates was observed compared to EYPC-SUVs (Table 1, entries 8 and 15−17).

The presence of sterols (e.g., cholesterol in eukaryotic cells or ergosterol in the cell membranes of fungi) decreases the fluidity of a lipid bilayer above the gel-to-liquid crystalline phase transition temperature (EYPC: $T_m = 4$ °C).[21] The effect of sterols in EYPC-membranes on ion transport rates thus indicates whether molecular motion is involved in the mechanisms of action of the corresponding ionophores. Although the observed effects were small, the increased activity of polyol **1** in the presence of both cholesterol (1.43-fold) and ergosterol (1.56-fold) disfavors a mobile carrier mechanism and favors a channel mechanism.[7] Control experiments showed that incorporation of **1** at 40 °C for 15−30 min before the application of the pH gradient does not significantly change the observed weak selectivity. The incorporation mechanism of **1** (Figure 5) is thus apparently independent of the membrane fluidity, and the observed differences in rate arise from an ion transport ability. In contrast to AmB,[5] the activity of **1** is not dramatically altered by the presence of sterols, indicating that specific molecular interactions of monomeric or self-assembled **1** with sterols are unlikely.

The molecular basis of the 4.26-fold increase in activity of the uncharged polyol **1** in negatively charged POPG-SUVs compared to EYPC-SUVs is unclear. Judging from the increased concentration dependence in POPG, as compared to EYPC, a relatively high percentage of membrane-bound **1a** may account at least in part for the observed high activity in POPG. Further studies on this mechanistically unusual example of bilayer membrane recognition are ongoing and may have potential pharmacological significance.

Absence of Membrane Defects. The lytic ability of polyol **1** was evaluated using uniformly sized EYPC-SUVs loaded with self-quenching 5(6)-carboxyfluorescein (CF, Figure 7).[22] Addition of the bee toxin melittin (1 μM) resulted in rapid release of CF through the induced membrane defects as determined by the increase of CF emission as a function of time.[23] No change

(20) Since EYPC mainly consists of 1-palmitoyl- and 2-oleoyl-PC, POPG was selected for the comparison with EYPC.

(21) (a) Vilceze, C.; McMullen, T. P. W.; McElhaney, R. N.; Bittman, R. *Biochim. Biophys. Acta* **1996**, *1279*, 235. (b) Mabrey, S.; Sturtevant, J. M. *Biochemistry* **1978**, *17*, 3862. (c) Demel, R. A.; De Kruijff, B. *Biochim. Biophys. Acta* **1976**, *457*, 109.

(22) Rex, S. *Biophys. Chem.* **1996**, *58*, 75.

(23) (a) Juvvadi, P.; Vunnam, S.; Merrifield, R. B. *J. Am. Chem. Soc.* **1996**, *188*, 8989. (b) Dempsey, C. E. *Biochim. Biophys. Acta* **1990**, *1031*, 143.

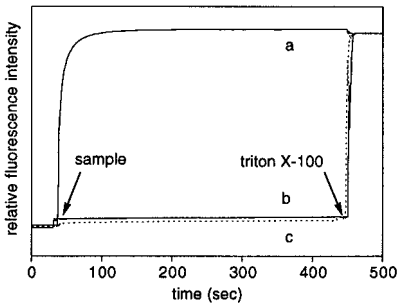

Figure 7. Change in fluorescent intensity ($(I_t - I_0)/(I_\infty - I_0)$, $\lambda_{em} = 514$ nm, $\lambda_{ex} = 492$ nm) of EYPC vesicle-entrapped CF (50 mM) as a function of time in the presence of (a) 1 μM melittin, (b) 20 μM **1**, and (c) 1 μM gramicidin D.

in emission after addition of the detergent triton X-100 indicated that all vesicles were entirely lysed by melittin (Figure 7, curve a). In contrast, the ion channel-forming gramicidin D[3] (1 μM) did not mediate significant CF release (curve c). The nearly identical curves for gramicidin D (1 μM) and polyol **1** (20 μM, curve b) demonstrate that **1**, apparently in contrast to AmB,[5b] does not act as a defect inducer in EYPC-SUVs.

Structural Studies by Circular Dichroism. In order to study the aggregation behavior of **1** by circular dichroism (CD), chiral polyol (***R*)-1** (Figure 2A), having (*R*)-configuration at all carbons connected to the secondary OH groups, was synthesized following the previously reported procedure for the diastereomeric mixture of **1**.[1] Since the ion transport activities of (***R*)-1** and its diastereomeric mixture were the same within experimental error, (***R*)-1** is also referred to as **1** in experiments where stereochemistry did not alter the results.

In MeOH, in which polyol **1** is most soluble, and in TFE, the CD spectrum of (***R*)-1** gave no distinct signal, indicating the absence of self-assemblies (Table 2). In the nonpolar solvent methylene chloride, a bisignate CD curve centered roughly around the absorption maximum at 324 nm is followed by a weaker positive Cotton effect at 281 nm ($\Delta\epsilon = +17$, Figure 8). In octanol, the bathochromic, bisignate CD curve broadens and decreases ($A = -28$) relative to methylene chloride ($A = -90$), and the positive Cotton effect at 267 nm increases ($\Delta\epsilon = +38$). In water, a small, split CD Cotton effect centered around the long wavelength absorption maximum is observed ($A = -5.8$), but there is no positive CD Cotton effect at shorter wavelength as in nonpolar solvents.

The split CD Cotton effects observed in water, octanol, and methylene chloride, having relatively large amplitudes of up to $A = -90$, are characteristic for the interaction of the excited states of two chromophores close in space and thus diagnostic for supramolecular structures of (***R*)-1**.[24] The concentration dependence of the amplitudes in all solvents corroborates this interpretation. The difference in shape indicates that three different suprastructures of (***R*)-1** are formed in these solvents. The larger amplitudes in nonpolar solvents are consistent with suprastructures in which the chiral centers in the polar side chains are tightly packed and surrounded by the benzene rings. A loose packing of the chiral centers placed on the surface of the self-assembled oligophenylene rods may account for the comparably small amplitude observed in water (Figure 5, structure **1b**). The negative sign of the split CD Cotton effect implies for all observed self-assemblies a negative sense of twist between the coupling transition moments.

Although the unfavorable signal-to-noise ratio of weak CD signals, such as (***R*)-1** in water, lessens the accuracy of the measurements, the almost identical CD curves ($A \approx -5.8$) obtained in the presence or absence of EYPC-SUVs allow valid qualitative interpretation (Figure 8, Table 2). The curves were taken under conditions identical to those of the flux assays. The concentration dependence of the activity of **1** led to the conclusion that more than 84% of **1** is inactive at 20 μM. The virtually unchanged CD curves with or without EYPC-SUVs prove that this inactive part of (***R*)-1** is a self-assembly similar or identical to the one formed in water (**1b** in Figure 5). Moreover, a suprastructure similar to that in octanol or methylene chloride is not present in EYPC-bilayers, since the strong positive Cotton effect around 280 nm in "nonpolar" suprastructures of **(*R*)-1** ($\Delta\epsilon \geq +17$) would also be detectable if less than 16% (but more than ~3%) of **(*R*)-1** accounts for that signal. Although there is no definitive evidence, these results strongly support the previous conclusion that the active structure of rigid rod polyol **1** is monomeric (**1a** in Figure 5).

Structural Studies by Fluorescence Spectroscopy. Oligo(*p*-phenylene)s are photostable fluorophores with high quantum yield, short fluorescence decay times, relatively large Stokes shifts, and a broad spectral region of fluorescence.[6p] With increasing length, absorption and emission maxima undergo bathochromic shifts, and both intensities increase. The fluorescence quantum yield of polyol **1** in water was determined according to standard methods using quinine bisulfate in 0.1 N sulfuric acid as a reference.[25] The obtained value of $Q_f = 0.87$ was higher than the reported quantum yields for substituted quaterphenyls (0.69−0.80).[6p] The relative emission intensity of **1** decreases upon self-assembly (judged by CD, Table 2). TFE did not follow this trend (0.26, $A \approx 0$). Presumably due to the short fluorescence life time, polarization of fluorescence (using polarized light for excitation) did not significantly change upon self-assembly of **1** as detected by CD ((***R*)-1**) and a decrease in fluorescence emission intensity.

Fluorescence Resonance Energy Transfer. Fluorescence resonance energy transfer (FRET) methods[26] have recently received increasing attention as promising and powerful tools in membrane research.[27] In order to study the binding of polyol **1** to EYPC-bilayers, BODIPY FL was selected as an acceptor fluorophore (Figure 9, spectra c and d). EYPC-SUVs were doped with 0.14 mol % membrane probes carrying BODIPY analogs attached either to the lipid head group (BODIPY FL DHPE) or to the terminus of a fatty acid chain segment (β-BODIPY FL C12-HPC). A Föster energy transfer radius of $R_0 = 36 \pm 2$ Å was estimated from the integration of the spectral overlap between BODIPY excitation and polyol **1** emission spectra ($J = 1.512 \times 10^{-14}$ cm^6/M) and Q_f(**1**) = 0.87.[26a] The additional peak at 510 nm in the emission spectrum of polyol **1** (and **2**) in the presence of BODIPY-labeled vesicles clearly demonstrates FRET from the polyol donor to the BODIPY acceptor and thus binding of octamer **1** (and **2**) to EYPC-bilayers (Figure 9, spectrum e). However, no differences were observed in the transfer efficiencies from **1** or **2** to BODIPY-labels located at the membrane/water interface or in the middle of the hydrophobic part of the bilayer. A time course of binding and intervesicular transfer of polyols followed by an intensity change

(24) (a) Nakanishi, K.; Berova, N. In *Circular dichroism: principles and applications*; Nakanishi, K., Berova, N., Woody, R. W., Eds.; VCH: Weinheim, 1994; p 361. (b) Matile, S.; Berova, N.; Nakanishi, K. *Chem. Biol.* **1996**, *3*, 379.

(25) (a) Parker, C. A.; Rees, W. T. *Analyst* **1960**, *85*, 587. (b) Melhuish, W. H. *J. Phys. Chem.* **1961**, *65*, 229.

(26) (a) Yang, M.; Millar, D. P. *Methods Enzymol.* **1997**, *278*, 417. (b) Stryer, L. *Annu. Rev. Biochem.* **1978**, *47*, 819.

(27) (a) Gonzalez, J. E.; Tsien, R. Y. *Chem. Biol.* **1997**, *4*, 269. (b) Keller, R. C. A.; Silvius, J. R.; De Kruijff, B. *Biochem. Biophys. Res. Commun.* **1995**, *207*, 508. (c) Schwarz, G.; Beschiaschvili, G. *Biochim. Biophys. Acta* **1989**, *979*, 82.

Table 2. UV−Vis, CD, and Fluorescence Data of Rigid Rod Polyol **1** ((***R***)-**1**)

	$\epsilon(\lambda^a_{max})^a$	$\Delta\epsilon(\lambda^a_{max})^b$	A^c	rel intens $(\lambda^e_{max})^d$
CH_2Cl_2	35 960 (324)	−68 (339), +22 (306), +17 (281)	−90	0.17 (412)
octanol	32 500 (322)	−8.0 (338), +17 (sh., 301), +38 (267)	−25	0.26 (390)
TFE	31 440 (312)	nd[g]	0	0.29 (379)
MeOH	46 124 (316)	nd[g]	0	1.00 (382)
H_2O[e]	28 640 (320)	−4.0 (339), +1.8 (314)	−5.8	0.42 (389)
EYPC[f]	28 640 (320)	−4.0 (339), +1.8 (314)[h]	−5.8[h]	0.51 (389)[i]

[a] Absorption data, in L mol^{-1} cm^{-1} (nm). [b] Differential dichroic absorption, in L mol^{-1} cm^{-1} (nm), measured at 20 μM; all observed CD signals are concentration dependent. [c] CD amplitude, L mol^{-1} cm^{-1}, at 20 μM; all observed amplitudes are concentration dependent. [d] Fluorescence emission data (nm); intensities are relative to that in MeOH; measured at 2.5 μM. [e] 100 mM NaCl, 100 mM HEPES, pH 7.0. [f] Sample added to EYPC vesicles (0.27 mM) in 100 mM NaCl, 100 mM HEPES, pH 7.0. [g] Not distinct. [h] Decreased CD signal observed in some experiments. [i] Occasional increase in intensity of emission observed in some experiments.

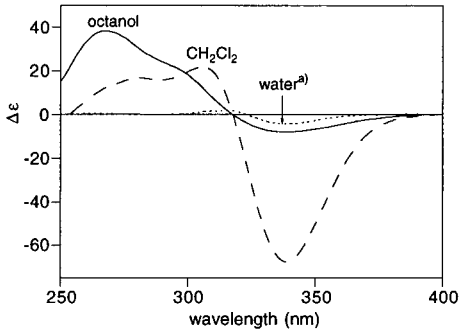

Figure 8. CD spectra of **(*R*)-1** in methylene chloride, octanol, and water. (a) Octamer **(*R*)-1** in water, buffer, and vesicle suspension gave spectra which are identical within experimental error.

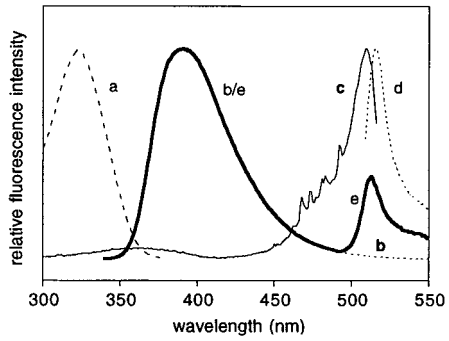

Figure 9. Spectral properties of octamer **1** and BODIPY FL DHPE: (a) excitation spectrum of **1** (emission at 389 nm); (b) emission spectrum of **1** (excitation at 320 nm); (c) excitation spectrum of BODIPY FL DHPE (emission at 530 nm); (d) emission spectrum of BODIPY FL DHPE (excitation at 470 nm); (e) emission spectrum of **1** added to BODIPY-labeled EYPC vesicles (excitation at 300 nm).

in the FRET signal (510 nm, excitation at 300 nm) fully agreed with the result obtained by fluorescence quenching methods (*vide infra*).

Fluorescence Quenching. Binding and orientation of the polyphenylenes **1** and **2** to EYPC-bilayers were further investigated by using spin-labeled lipids 1-palmitoyl-2-stearoyl (5-DOXYL)-*sn*-glycero-3-phosphocholine (5-DOXYL-PC) and 1-palmitoyl-2-stearoyl (12-DOXYL)-*sn*-glycero-3-phosphocholine (12-DOXYL-PC). Fluorescence quenching techniques are widely used to determine distribution of a fluorophore in (bio)-membranes.[28] The major advantage of these methods over FRET is the short effective distance between the quencher and the fluorophore (∼12 Å with spin label), which allows the determination of not only binding behavior but also the approximate location of the fluorophore in the membrane. The relative emission intensities of **1** and **2** in the presence of 5- or 12-DOXYL-PC are shown in Figure 10A. Compared to emission intensity in the nonlabeled vesicle (I_0), the fluorescence of octamer **1** was quenched about 40% by both 5-DOXYL-PC

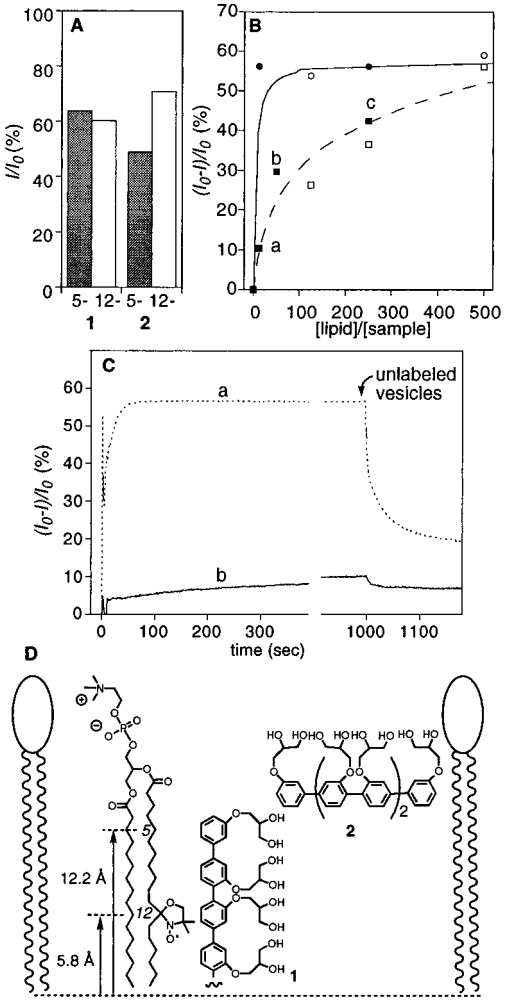

Figure 10. Quenching of the fluorescence of **1** and **2** by 5- or 12-DOXYL-PC labeled vesicles. (A) Relative emission intensities (I/I_0, %) of octamer **1** and hexamer **2** at 1 μM, with 0.25 mM of 5-DOXYL-PC and 12-DOXYL-PC labeled vesicles. I_0 represents the emission intensity of the samples with unlabeled vesicles. (B) Quenching efficiencies of **1** (squares) and **2** (circles) with 5-DOXYL-PC labeled vesicles**.** Data were obtained with various concentrations of **1** or **2** in the presence of 0.25 mM vesicle suspension (filled) or with 1 μM of **1** or **2** in the presence of various concentrations of vesicles (open). Measured with (a) 20 μM of **1**, (b) 5 μM of **1**, or (c) 1 μM of **1** with 0.25 mM of lipid. (C) Time course of the quenching with 20 μM polyols **1** or **2** in the presence of 0.25 mM of 5-DOXYL-PC labeled vesicles, followed by the addition of unlabeled EYPC vesicles (0.25 mM). (a) **2** with 5-DOXYL-PC labeled vesicles. (b) **1** with 5-DOXYL-PC labeled vesicles. (D) Schematic presentation of the orientation of octamer **1** and hexamer **2** in EYPC bilayers.

(28) (a) Abrams, F. S.; London, E. *Biochemistry* **1992**, *31*, 5312. (b) Ladokhin, A. S. *Methods Enzymol.* **1997**, *278*, 462. (c) Yeager, M. D.; Feigenson, G. W. *Biochemistry* **1990**, *29*, 4380. (d) Chattopadhyay, A.; London, E. *Biochemistry* **1987**, *26*, 39.

and 12-DOXYL-PC labeled vesicles, while that of hexamer **2** was quenched more strongly by 5-DOXYL-PC (∼55%) than by 12-DOXYL-PC (30%). The latter results indicate that hexamer **2** stays close to the surface, and most probably lies parallel to the membrane surface at the membrane/water interface (Figure 10D). Parallax analysis[28a] gave the distance between the hexamer and the center of the bilayer to be 15.5 Å, which is consistent with this model. On the other hand, almost identical quenching efficiencies with 5-DOXYL-PC and 12-DOXYL-PC at 1 μM unambiguously corroborate the transmembrane orientation of octamer **1** (Figure 10D).

Binding[29] and intervesicular transfer of **1** and **2** were assessed by studying the time course of quenching under conditions identical to those used in the flux assays (Figure 10C). Since membrane incorporation usually occurs in milliseconds,[27c,30] the fast incorporation observed for hexamer **2** is as expected (curve a). The ∼50% decrease in quenching percentage upon addition of unlabeled vesicles indicates unhindered intervesicular transfer and statistical distribution of **2** among different vesicle populations. In contrast, addition of unlabeled vesicles reduced the quenching percentage of octamer **1** by about 25%, indicating partially irreversible binding of **1** to EYPC bilayers. These findings, namely, reversible binding of **2** but partially irreversible incorporation of **1**, were fully corroborated by the analogous FRET experiments (not shown). It should be noted that, in the case of (partially) irreversible "all or none"-type[15] incorporation as observed for octamer **1**, the intervesicular transfer rate is thought to further limit the observed overall ion flux rates. In other words, the channel formation rate[7] in nonpermealized vesicles may lower the apparent transport activity of **1**, but presumably not of **2**.[15]

As shown in Figure 10C, the quenching efficiency observed with **1** was significantly lower than that with **2**, indicating much inferior incorporation of **1** into the lipid bilayer at 20 μM. In order to estimate the binding profiles of octamer **1** and hexamer **2**, the quenching efficiencies were measured at various lipid and sample concentrations (Figure 10B). Varying the sample or lipid concentration essentially did not alter the binding tendency. Hexamer **2** showed virtually the same percentage of quenching by 5-DOXYL-PC (∼55%) at all measured lipid/sample ratios. In contrast, octamer **1** showed a highly concentration-dependent binding behavior which is fully consistent with the concentration dependence of its activity. With respect to the different binding behavior of **1** and **2**, the length dependence of the transport activities should thus be more pronounced than previously concluded.[1] Namely, if we assume that the percentage of quenching is proportional to the incorporation ratio,[29] 5.5 times more of hexamer (55%) than octamer (10%) should account for overall activity at 20 μM (Figure 10C). Judging from the apparent 3 times higher transport activity of **1** compared to **2** at 20 μM,[1] *the membrane-spanning fraction of octamer **1** must thus be 16.5 times more active than hexamer **2**.*

Conclusions

Our studies on the mode of action of rigid rod-shaped polyol **1** allow us to propose conceivable mechanisms of incorporation and transport, and a model for the active structures (Figures 2 and 5). It is important to reiterate that the results of the above mechanistic and structural studies are comparable because all experiments were conducted under the same or comparable conditions. Therefore, the results discussed above[31] imply that rigid rod polyol **1** acts as a presumably unimolecular, proton-selective ion channel in SUVs.[7] Apparently, only a minor fraction of polyol **1** adopts the active structure **1a** at 20 μM, while the bulk of **1** exists as an inactive self-assembly (**1b** in Figure 5). At lower concentrations, the relative amount of the active conformer increases.

There is unambiguous evidence that active, presumably monomeric octamer **1** adopts a transmembrane orientation as proposed,[1] and the match of the length of the rigid rod molecules with the thickness of the lipid bilayer is indeed critical for length-dependent activity as well as transmembrane binding. The pronounced proton selectivity is best explained with the active conformer **1a** (Figure 2B): The hydroxyl groups form a transmembrane HBC which is partially covered by the hydrophobic C_3-chains and the oligophenylene rod. The model conformer **1a** further contains a central "tunnel" of diameter ca. 4 Å, equipped with ionophoric oxygens and aromatic rings which may account for the comparably slow and weakly selective transport of metal cations. We believe that these findings provide a solid, rational basis for further research on the chemical, biological, and pharmacological[32] significance of unprecedented nonpeptide HBC-proton channel models[11] as well as alternative rigid rod-shaped analogs which act in a length-dependent manner and apparently recognize negatively charged bilayer membranes.

Experimental Section

General Procedures. UV−vis spectra were recorded on a Hewlett-Packard 8452A diode array spectrophotometer and reported as ϵ_{max} [L mol^{-1} cm^{-1}] (λ_{max} [nm]) (Table 2). CD-spectra were recorded on a Jasco J-710 spectropolarimeter and reported as $\Delta\epsilon_{max}$ [L mol^{-1} cm^{-1}] (λ_{max} [nm]) (Table 2). Fluorescence spectra were recorded on FluoroMax-2 (Jobin Yvon-Spex). Both emission and excitation spectra were corrected using maker-supplied correction factors.

Egg yolk phosphatidylcholine (EYPC), 1-palmitoyl-2-oleoyl-*sn*-glycero-3-[phospho-*rac*-(1-glycerol)] (sodium salt) (POPG), 1-palmitoyl-2-stearoyl (5-DOXYL)-*sn*-glycero-3-phosphocholine (5-DOXYL-PC), and 1-palmitoyl-2-stearoyl (12-DOXYL)-*sn*-glycero-3-phosphocholine (12-DOXYL-PC) were purchased from Avanti Polar Lipids. 8-Hydroxypyrene-1,3,6-trisulfonic acid, trisodium salt (HPTS), 5(6) carboxyfluorescein (CF), BODIPY FL DHPE, and β-BODIPY FL C12-HPC were from Molecular Probes. Melittin, gramicidin D, valinomycin, detergents, all salts, and buffers were of the best grade available from Sigma and used without further purification. Polyol **(*R*)-1** was synthesized following the previously reported procedure for the diastereomeric mixture of **1** using (*R*)-(−)-(2,2-dimethyl-1,3-dioxolan-4-yl)methyl *p*-toluenesulfonate (Aldrich) instead of the racemic mixture.[1]

Vesicle Preparation. Small unilamellar vesicles (SUVs) were prepared by the dialytic detergent removal method using Mini Lipoprep

(29) Complete binding usually does not result in complete quenching.[28c] The quenching percentage is thus not equivalent to the incorporation ratio. However, the observed similar quenching efficiencies with various concentrations of **1** or **2** at the high [lipid]/[sample] ratios indicate that the maximal quenching percentages are similar (data not shown). It is thus reasonable to use the efficiencies as relative incorporation values.

(30) Driessen, A. J. M.; van den Hooven, H. W.; Kuiper, W.; van de Kamp, M.; Sahl, H.-G.; Konings, R. N. H.; Konings, W. N. *Biochemistry* **1995**, *34*, 1606.

(31) (1) A rate increase with decreasing membrane fluidity, (2) transmembrane orientation (length-dependent activity), (3) poor selectivity for group 1A cations (Eisenmann sequence II), divalent cations, and anions, (4) significant proton selectivity, (5) absence of lysis, (6) absence of "nonpolar" self-assemblies, and (7) a concentration dependence profile are in full agreement with an ion channel mechanism. (1)−(3) disfavor a mobile carrier mechanism, (4)−(5) disfavor the induction of a membrane defect, and (6) and (7) disfavor the presence of active "barrel-stave"-type self-assemblies.

(32) Proton channel models are proposed to have important applications in reversal of multidrug resistance of cancer cells, viral uncoating, immunotoxin potentiation, control of bacterial toxins, immune response, prion replication, malaria, and intralysosomal microorganisms. See: (a) Dubowchik, G. M.; Padilla, L.; Edinger, K.; A., F. R. *Biochim. Biophys. Acta* **1994**, *1191*, 103. (b) Dubowchik, G. M.; Padilla, L.; Edinger, K.; Firestone, R. A. *J. Org. Chem.* **1996**, *61*, 4676. See also ref 2i.

(Sialomed) which gives reproducibly uniformly sized vesicles. We and others[15,22] have noticed that ion transport activities are significantly altered by the size of the vesicles used; variations in vesicle size are an important parameter which can reduce the reproducibility of the measurements.

EYPC Vesicles. A solution of EYPC (50 mg, 66 μmol) in ethanol (50 μL) was mixed with sodium cholate (22.4 mg, 52 μmol) and 950 μL of 100 mM HEPES (pH 7.0), 100 mM saline (NaCl unless otherwise indicated) buffer containing 0.1 mM HPTS (buffer A). The resulting clear solution was dialyzed against 150 mL of buffer A at room temperature (rt) for 15 h and then against 1 L of the same buffer without HPTS (buffer B) for 4 h. All dialyses were carried out in the dark. Extravesicular HPTS was further removed by gel filtration (Sephadex G-50, 1 × 27 cm) using buffer B. The vesicle suspension was diluted with buffer B to 6 mL to give 10 mM vesicle stock solution.

POPG Vesicles. POPG (50 mg, 65 μmol) and sodium cholate (22.4 mg, 52 μmol) were dissolved in 300 μL of $CHCl_3$/EtOH (2/1). The mixture was dried slowly with a rotary evaporator to form a thin film and then put under vacuum for 1 h. The lipids were rehydrated with buffer A (1 mL). The resulting mixture was dialyzed against 150 mL of buffer A for 18 h at rt and then against 1 L of buffer B for 4.5 h. Gel filtration of the suspension yielded a 10 mM vesicle stock solution.

EYPC/Cholesterol and EYPC/Ergosterol Vesicles. A solution of EYPC (50 mg, 66 μmol) in ethanol (50 μL) was mixed with sodium cholate (22.4 mg, 52 μmol), cholesterol (6.4 mg, 16 μmol), or ergosterol (6.5 mg, 16 μmol), and 950 μL of buffer A at 40 °C. The resulting suspension was dialyzed against 150 mL of buffer A at 40 °C for 4 h and at rt for 15 h and then against 1 L of buffer B for 4 h at rt. Extravesicular HPTS was further removed by gel filtration using buffer B. The vesicle suspension was diluted to 6 mL to give a 10 mM vesicle stock solution.

Transport Studies (General Procedure). The vesicle suspension (50 μL) was placed in a cell and diluted with the appropriate buffer solution (1.95 mL). To the gently stirred mixture 2 M NaOH(aq) (40 μL) was added through an injector port to establish a pH gradient of 0.6 pH unit. In some experiments, 1.2 μM valinomycin in DMSO (20 μL) was added next. Then, a solution of the appropriate channel-forming molecule (40 μL of 1 mM **1** in methanol for most experiments, 0.25 mM **1** in methanol (40 μL) for Table 1, entry 5, 50 μM **1** in methanol (40 μL) for entry 6) was injected. Finally, vesicles were lysed by addition of triton X-100 (10% aqueous solution, 50 μL). The fluorescence emission intensity was monitored at 510 nm (excitation at 460 nm) during an entire experiment period and recorded as a function of time. Control experiments revealed that the sequence of addition (NaOH and then **1** or **1** and then NaOH) as well as the incorporation time given for **1** before adding NaOH does not significantly change the activity of **1**.

Salt Concentrations in Selectivity Experiments. The K^+/H^+ selectivity was determined with the following salt concentrations (Figure 4). Curve a: 100 μL of vesicle stock solution (intravesicular = 100 mM NaCl + 0.05 mM KCl, extravesicular = 100 mM KCl) was diluted with 1.9 mL of buffer containing 100 mM KCl, giving a Nernst potential ($\psi = -58$ mV × log($[K^+_{out}]/[K^+_{in}]$)) of $\psi = +190$ mV. Curves b−d: 100 μL of vesicle stock solution (intravesicular = extravesicular = 100 mM KCl) and 1.9 mL of buffer with 100 mM KCl; $\psi = 0$ mV. Curves e and f: 100 μL of vesicle stock solution (intravesicular = 100 mM KCl, extravesicular = 100 mM NaCl + 0.05 mM KCl) and 1.9 mL of buffer with 0.05 mM KCl + 100 mM NaCl; $\psi = -190$ mV. The following salt distributions were used for the experiments shown in Table 1, entries 1 and 7−14: 50 μL of vesicle stock solution (intravesicular = extravesicular = 100 mM NaCl) was diluted with 1.95 mL of buffer containing 100 mM M_nX_y as indicated in Table 1. With all salt distributions, practically no ion transport was observed without octamer **1** and/or valinomycin.

Data Analysis. Normalized kinetic curves $[(I_t - I_0)/(I_\infty - I_0)]$ as shown in Figure 4 were calculated using KaleidaGraph V.2.3. Comparable initial first-order rate constants were obtained using normalized curves. It is well known that activities determined by flux assays may differ significantly when taken on different days depending on the various parameters involved.[2g] However, in agreement with the observations reported by Fyles and co-workers,[2g] an error of $\leq \pm 5\%$ was observed during experimental sequences performed on the same day with identical material. In the case of small differences in rate constants, the observed sequences were reproducible. For this reason, experimental data were usually compared to a value obtained using EYPC, $[Na^+_{in}] = [Na^+_{out}] = 100$ mM, measured during each sequence of experiments (Table 1, entry 1). The further calculated relative rates k/k_{Na^+} allow comparison with other experimental sequences (Table 1).

Leakage Assay. SUVs were prepared in a manner similar to that above. EYPC (50 μL of stock solution in EtOH, 66 μmol) and sodium cholate (22.4 mg) were dissolved in a buffer containing CF (950 μL; 50 mM CF, 10 mM HEPES, 10 mM NaCl, pH 7.4).[22] The resulting solution was dialyzed against 25 mL of the same buffer at rt for 8 h, and then against 1 L of the osmotically balanced buffer without CF (buffer C: 10 mM HEPES, 107 mM NaCl, pH 7.4) for 14 h in the dark. After the removal of extravesicular CF by gel filtration, the vesicle suspension was diluted to give a 10 mM stock solution. The vesicle stock solution (50 μL) was diluted with 1.95 mL of buffer C in a cell. To a gently stirred solution was added the appropriate sample solution (40 μL of 1 mM octamer solution in MeOH, 20 μL of 0.1 mM gramicidin D solution in DMSO, or 20 μL of 0.1 mM melittin solution in water). The fluorescence intensity change at 514 nm (excitation 492 nm) was recorded as a function of time. Finally 100% release of CF was achieved by the addition of triton X-100 (1.2%, 50 μL).

Fluorescence Resonance Energy Transfer Experiments. A solution of BODIPY FL DHPE (100 μg, 94 nmol), EYPC (50 μL of stock solution in EtOH, 66 μmol), and sodium cholate (22.4 mg) in 950 μL of buffer B was dialyzed against 1 L of the same buffer for 7 h in the dark. The resulting vesicle suspension was diluted with the same buffer to give a lipid concentration of 6 mM. SUVs labeled with β-BODIPY FL C12-HPC were prepared in an identical manner. The vesicle suspension (100 μL) was diluted with 1.9 mL of buffer B, and the solution of octamer (10 μL of **1**, 0.1 mM MeOH solution) was added. After ~20 min, emission spectra of octamer **1** were recorded (excitation at 300 nm). The background fluorescence (labeled lipids in buffer) was subtracted from the apparent emission spectra for the calculation of the efficiency of energy transfer.

Fluorescence Quenching Experiments. A solution of 5- or 12-DOXYL-PC (2 mg, 2.3 μmol), EYPC (18 μL of stock solution in EtOH, 24 μmol), and sodium cholate (8 mg) in 400 μL of buffer B was dialyzed against 400 mL of the same buffer for 6 h at rt. The resulting vesicle suspension was diluted with the same buffer to give a 10 mM stock solution. Samples were added to the appropriate concentration of vesicle suspension in buffer B. Emission intensities (I) were measured at 1, 5, or 20 μM of **1** or **2** in the presence of 0.125, 0.25, 0.5, or 1 mM 5-DOXYL-PC or 12-DOXYL-PC labeled vesicles, and compared to the emission intensities in the same concentration using unlabeled lipid (I_0). Octamer **1** fluorescence was measured after ~20 min of incubation for reproducible results. Excitation and emission wavelengths used for measurements were $\lambda_{ex} = 328$ nm and $\lambda_{em} = 390$ nm for **1** and $\lambda_{ex} = 323$ nm and $\lambda_{em} = 384$ nm for **2**.

Acknowledgment. We thank NIH (Grant GM56147-01), the donors of the Petroleum Research Fund, administered by the American Chemical Society, Suntory Institute for Bioorganic Research (SUNBOR Grant), and Georgetown University for support of this work. Further support by NSF (Grant CHE-9601976), through the Georgetown Molecular Modeling Center, and a Fulbright Fellowship (B.G.) are gratefully acknowledged.

JA973126D